buildings

MDPI

Article

The Mechanical Properties and Mechanisms in Contact-Hardening Behavior of Silica-Alumina Mine Solid Waste

Baojun Cheng [1,2], Xiaowei Gu [1,*], Haoyue Hu [2], Yaning Kong [2,*] and Pengyu Huang [2]

[1] School of Resources and Civil Engineer, Northeastern University, Shenyang 110819, China; 2190072@stu.neu.edu.cn
[2] China West Construction Building Materials Science Research Institute, Chengdu 610221, China; 20162999@cqu.edu.cn (H.H.); 20155665@cqu.edu.cn (P.H.)
* Correspondence: guxiaowei@mail.neu.edu.cn (X.G.); kongyaning1224@126.com (Y.K.)

Abstract: There are some limitations in the application of tuff powder as a supplementary cementitious material (SCM). Exploring its feasibility in new fields will consume a large amount of silica-alumina mine solid wastes. This study has investigated the mechanical properties and mechanism in contact-hardening of tuff powder with a method of compression molding. The compressive strength of specimens was tested, and the X-ray diffraction (XRD), thermogravimetric analysis (TG), scanning electron microscopy (SEM), and Mercury intrusion porosimetry (MIP) methods were used to reveal the mechanism of contact-hardening of tuff powder from a micro-perspective. The results indicated that the compressive strength of specimens was higher when activated by sodium hydroxide compared to calcium hydroxide. Compared to calcium hydroxide, the compressive strength of TFS20 and TFF20 activated by sodium hydroxide was improved by 20% and 23%, respectively. The hydration degree of tuff powder was very low, with a water–cement ratio (w/c) of 0.15, while the hydration degree of coal gangue powder was higher. The results of TGA and SEM indicated that the sodium hydroxide had a better activating effect on slag and fly ash. Therefore, more C-S-H gels were generated in those samples activated by sodium hydroxide. Furthermore, the structure of samples was more compacted, and there was a reduction of porosity by 10% and 11% for TFS20 and TFF20, respectively, especially the proportion of harmful pores.

Keywords: solid wastes; contact-hardening; alkali-activated; compressive strength; microstructure

Citation: Cheng, B.; Gu, X.; Hu, H.; Kong, Y.; Huang, P. The Mechanical Properties and Mechanisms in Contact-Hardening Behavior of Silica-Alumina Mine Solid Waste. *Buildings* **2024**, *14*, 922. https://doi.org/10.3390/buildings14040922

Academic Editor: Abdelhafid Khelidj

Received: 18 February 2024
Revised: 12 March 2024
Accepted: 22 March 2024
Published: 27 March 2024

1. Introduction

Against the background of carbon peak and carbon neutrality, there are many challenging problems in the cement and concrete industries, such as high energy consumption and large carbon emissions [1]. The cement and concrete industries are reported to account for approximately 9–10% of global energy-related CO_2 emissions (including production, supply chain and disposal) [2]. Hence, it will have a significant impact on global energy consumption and carbon emissions that the cement and concrete industry is entering a "low-carbon" process.

So far, using less cement or replacing cement with supplementary cementitious materials (SCMs) have become the main methods to reduce carbon emissions in the cement and concrete industry [3,4]. In recent years, limestone calcined clay cement, which is a ternary system (clinker, calcined clay, limestone powder) mixed cement has been promoted in Europe and other places. This type of cement works through the pozzolanic effect, the reaction between alumina and carbonate and the filling effect of limestone powder [5]. Alkali slag cement has also been very popular in recent years [6,7], which is made by replacing cement clinker with 20% to 70% slag. Slag, which is used as the precursor of aluminosilicate, can continuously generate hydrated calcium silicate under the action of alkali activator. The greenhouse gas emissions during the production of alkali slag cement are

only 15% to 40% of those in the production of Portland cement [8]. Supersulfated cement is composed of at least 75% mineral powder, 5% to 20% calcium sulfate, and 0 to 5% alkali activator content of clinker [9]. Under the action of alkali activator, the silicon aluminum phase in mineral powder dissolves and reacts with calcium ion, sulfate ion, etc. in water to generate ettringite and C-(A)-S-H gel [10]. Compared to producing ordinary Portland cement, there is lower energy consumption and lower carbon emissions in supersulfated cement production.

Currently, China's mining solid waste reaches 70 billion tons [11], and it is being produced at a rate of 3 billion tons per year. The accumulation and storage of solid waste can cause serious environmental problems and resource waste. The silica-alumina mine solid wastes, which have a great utilization value, currently generally face problems such as the difficulty of activation, the association of the inert particle and the difficulty of component difference matching.

Tuff powder is a type of silica-alumina mine solid waste, which is mainly composed of SiO_2, Al_2O_3, and Fe_2O_3. At present, tuff powder is used as an SCM in many studies, but its pozzolanic activity remains a major limiting factor for its application. The pozzolanic activity is mainly related to the content of amorphous silica tetrahedra and alumina tetrahedra, as well as the degree of glass depolymerization [12,13] and phase separation structure [14], while in tuff powder it contains more low-temperature quartz and feldspar [15]. Scholars have conducted numerous studies on the improvement of tuff powder's pozzolanic activity. Liu [16] pointed out that its pozzolanic activity can be enhanced through thermal curing. Alternatively, calcining the tuff at 760 °C for 12 h can fully stimulate its pozzolanic activity [17]. Yu [18] found that NaOH and sodium silicate with applicable concentrations could activate tuff powder; the porosity was improved and the mechanical properties were significantly enhanced after 28 days of curing under high temperature conditions. In addition, some studies have shown that using tuff powder to replace some cement can reduce the hydration rate and total heat release in the early stage, but it has a slight adverse effect on the mechanical properties and durability in the later stage [16], and with the increase of its content, the porosity also increases [19]. Abali [20] also pointed out that the use of tuff powder can reduce the fluidity of the mixture and increase the setting time.

Coal gangue, another type of silica-alumina mine solid waste, has a negative impact on workability and compressive strength when used as coarse aggregate, because of its high water absorption and low strength [21,22]. Hence, the durability of concrete was influenced significantly, especially the frost resistance and carbonation resistance [23]. Therefore, coal gangue powder was investigated as an SCM. Research has shown that the pozzolanic activity of coal gangue powder can be improved to the maximum extent at a microwave temperature of 600–700 °C, which brought a good workability, too [24]. In addition, the mechanical properties of mortar prepared with it are greatly improved [25]. The physical adsorption capacity of coal gangue powder activated by the chemical insertion method or high temperature is improved, and the interaction ability with the matrix is enhanced. Therefore, the application of coal gangue powder in asphalt pavement can improve the high-temperature resistance and anti-aging performance [26]. Similarly, it also plays a positive role in self-healing cracks in asphalt mixtures and has a good self-healing effect under microwave heating conditions [27].

The low pozzolanic activity of tuff powder is its main drawback, and currently it generates huge energy consumption through high-temperature activation and other methods. Similarly, using coal gangue powder as an aggregate also faces many durability issues.

Obviously, searching for new application scenarios of tuff powder will achieve the goals of resource regeneration and environmental protection. Meanwhile, it will ultimately reduce carbon emissions in the construction industry and achieve sustainable development goals.

In 1970, the terminology "contact-hardening" was proposed by Glukhovsky [28]. It means that hydrated calcium silicate powder with high free energy can be compressed to form lightweight, high-strength and water-resistant artificial stone materials under the

driving force of room temperature pressure, immediately. Wang [23,29,30] pointed out that the moisture content, which is highly related to the drying conditions, is essential to the contact-hardening of C-S-H.

This study aims to study the mechanical properties and mechanism of contact-hardening of tuff powder and coal gangue with a method of compression molding, and explore its feasibility in new fields of application. This study reduced carbon emissions through the raw material approach, while also reducing energy consumption through molding methods. Since beneficial effects are caused by the application of slag, fly ash, silica fume, etc. in the field of building materials, this study will partially use them as substitutes for tuff powder. Meanwhile, the effects of two alkaline activators, calcium hydroxide and sodium hydroxide, on the mechanical properties and mechanism of action of the system are investigated.

2. Materials and Methods

2.1. Raw Materials

The tuff used in this experiment is from Henan province. It was ground with a ball mill for 30 min and then screened to obtain tuff powder. Its density is 2.65 g/cm^3 and its specific surface area is 585.8 m^2/kg. The 28-day activity index of tuff powder was tested according to pozzolanic materials used for cement production GB/T 2847-2022 [31], and was found to be 60%. The slag (S95) is produced from Chongqing, and the silica fume comes from Sichuan with a specific surface area of 22,205 m^2/kg. Fly ash of grade I is produced from Jiangyou, Sichuan, with a 28-day activity index of 101%. The coal gangue powder comes from Fuxin, Liaoning, with an activity index of 80% at 28 days. The chemical composition of the above materials is shown in Table 1 through X-ray fluorescence (XRF), which is closely related to the reactivity of different materials.

Table 1. Chemical composition of raw materials (wt%).

Materials	SiO_2	Al_2O_3	CaO	Fe_2O_3	MgO	SO_3	Na_2O	K_2O	LOI
Tuff powder (TP)	62.91	18.94	4.54	4.56	0.65	0.06	2.22	4.75	1.07
Furnace slag (FS)	29.67	20.52	32.74	0.33	6.82	2.38	0.42	0.80	6.22
Coal gangue (CG)	57.75	31.25	1.73	3.32	0.57	0.41	0.73	2.68	1.26
Silica fume (SF)	97.41	0.35	1.02	0.08	0.30	0.18	0.16	0.34	0.06
Fly ash (FA)	48.64	22.71	8.49	9.67	0.15	1.21	1.90	3.08	3.65

2.2. Preparation of Samples

Specimens were molded by an electro-hydraulic machine, which can achieve pressing and demolding functions. The mold is a cylindrical steel mold with a diameter and height of 5 cm. The specific steps are as follows: (1) load 220 g of stirred powder into the mold; (2) begin loading with a 200 KN pressure; (3) the load is maintained for 30–60 s for each specimen; (4) the formed specimen is demolded (Figure 1) and placed in a standard curing room for curing. The mixture proportions are shown in Table 2, where "-C" and "-N" are on behalf of specimens activated by calcium hydroxide and sodium hydroxide in the subsequent content of the article, respectively.

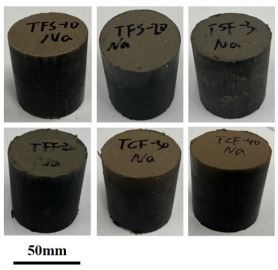

Figure 1. Appearance of specimens.

Table 2. Mixture proportions (wt%).

Sample	T	FS	SF	FA	CG	Water	$Ca(OH)_2$/NaOH [e]
TFS10 [a]	90	10	/	/	/	15	4/2
TFS20	80	20	/	/	/	15	6/3
TSF3 [b]	87	10	3	/	/	15	6/3
TFF20 [c]	80	10	/	10	/	15	6/3
TCF30 [d]	70	20	/	/	10	15	/3
TCF40	60	20	/	/	20	15	/3

[a] tuff powder and furnace slag; [b] tuff powder, furnace slag and silica fume; [c] tuff powder, furnace slag and fly ash; [d] tuff powder, furnace slag and coal gangue; [e] activated by $Ca(OH)_2$ or NaOH.

2.3. Testing Methods

2.3.1. Compressive Strength

The compressive strength of the specimens was examined after curing for 7 days and 28 days. The compressive strength, which was the average value of three specimens for each group, was calculated by Equation (1).

$$f_t = \frac{F_t}{s} \quad (1)$$

where f_t (MPa) is the compressive strength of specimen for t days, and F_t (KN) is the stress of the specimen for t days, and S (cm^2) is the area of compressed surface.

2.3.2. Micro-Analysis Techniques

The samples for micro-analysis were soaked in ethanol for 4 days at least to stop hydration when curing for 7 days and 28 days, and then the samples for X-ray diffraction (XRD) and thermogravimetry analysis (TGA) were ground to below 75 μm. XRD patterns were collected by a PANALYTICAL X-RAY TECHNOLOGY of aeris, using Cu Ka radiation and operating at 30 mA and 40 kV. Samples were scanned in the range of 2θ angle 5° to 70° within 6 min. TGA was carried out by an STD 650, heating from 30 °C to 1000 °C with a heating rate of 10 °C/min under a protective atmosphere of nitrogen. And the chemical bound water was calculated by Equation (2) [32]. In addition, a scanning electron microscope (ZEISS GeminiSEM 560 manufactured from Oberkochen, Germany) was used to examine the morphology of samples. Mercury intrusion porosimetry (AUTOPOREV 9620 manufactured from United States) was used to analysis the pore structure of samples.

$$BW = \frac{W_{40} - W_{550}}{W_{550}} \times 100\% \quad (2)$$

3. Results and Discussion

3.1. Compressive Strength

The compressive strength of the specimens, which were activated by calcium hydroxide, was examined after curing for 7 days and 28 days in Figure 2a. The increase in slag content from 10% to 20% led to an increase in compressive strength at 7 days. Compared to TFS10, TSF3 and TFF20 obtained a further increase in compressive strength because of adding 3% silica fume or 10% fly ash additionally, which might be related to the filling effect of silica fume [33] and the higher activity of fly ash compared to tuff powder. Specimens obtained a further increase in compressive strength of all groups as the curing days went by. Although the compressive strength exceeded 10 MPa after curing for 28 days, it is lower than that of traditional cementitious materials. This phenomenon might be related to the low content of amorphous C-S-H gel [29].

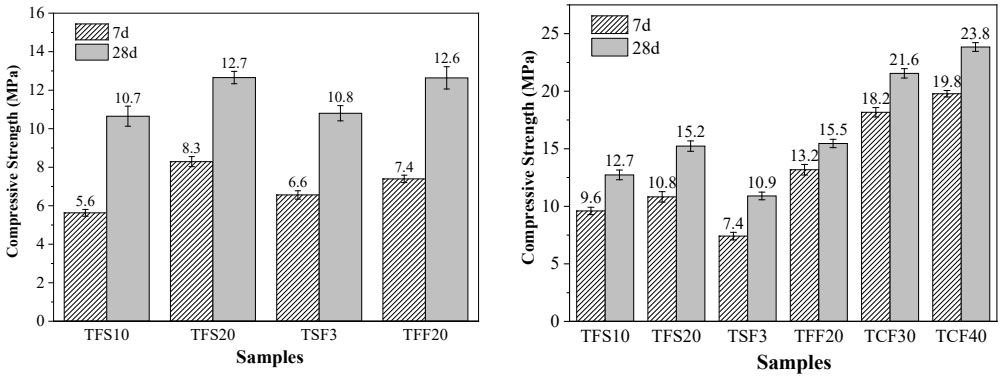

Figure 2. Compressive strength of samples after curing for 7 and 28 days. (**a**) Activated by calcium hydroxide. (**b**) Activated by sodium hydroxide.

To further improve the mechanical properties of each group, the alkaline activator was replaced with sodium hydroxide in the experiment, as sodium hydroxide had a greater solubility, which could release more OH^- compared to calcium hydroxide. Meanwhile, the influence of replacing part of the tuff powder with self-igniting coal gangue powder on the mechanical properties was investigated. The compressive strength results at 7 days and 28 days are shown in Figure 2b. The compressive strength of the same mixture proportion was improved after replacing the alkaline activator with sodium hydroxide, especially at 7 days. TFS10, TFS20 and TFF20 improved by 71%, 30% and 78%, respectively, at 7 days. But the alkaline activator had less impact on TSF3′s compressive strength at 7 and 28 days, which might be related to the fact that that the silica fume mainly played a filling role in this system. In addition, when tuff powder was partially replaced with self-igniting coal gangue powder, the mechanical properties improved significantly at 7 and 28 days. The 7-day compressive strength of TCF30 and TCF40 was 18.2 MPa and 19.8 MPa, respectively, which was higher than the 28-day compressive strength of other groups. At 28 days, the compressive strength was further improved, reaching 21.6 MPa and 23.8 MPa, respectively.

3.2. X-ray Diffraction

The mineral composition changes of all samples were tested at different ages, and the XRD patterns are shown in Figure 3. Figure 3a illustrates the mineral composition of the samples activated by calcium hydroxide after curing for 7 and 28 days. The compounds identified were quartz and albite ($2\theta = 27.913°$) from tuff powder [15], and calcite and portlandite ($2\theta = 18.063°$). The portlandite might be from the unreacted activator, and there was no difference between the results at 7 and 28 days. From the XRD patterns, there was no ettringite ($2\theta = 9.086°$) [34] or other hydration products in the samples after curing for 7 and 28 days. This result indicates that the degree of reaction between tuff powder and slag, silica fume and fly ash was relatively low with a method of compression molding at a w/c of 0.15. Meanwhile, hydration products could not be found in Figure 3b,c, even when using sodium hydroxide as an activator. There were only albite quartz and calcite from tuff powder, which meant that there was no ettringite or any other hydration products.

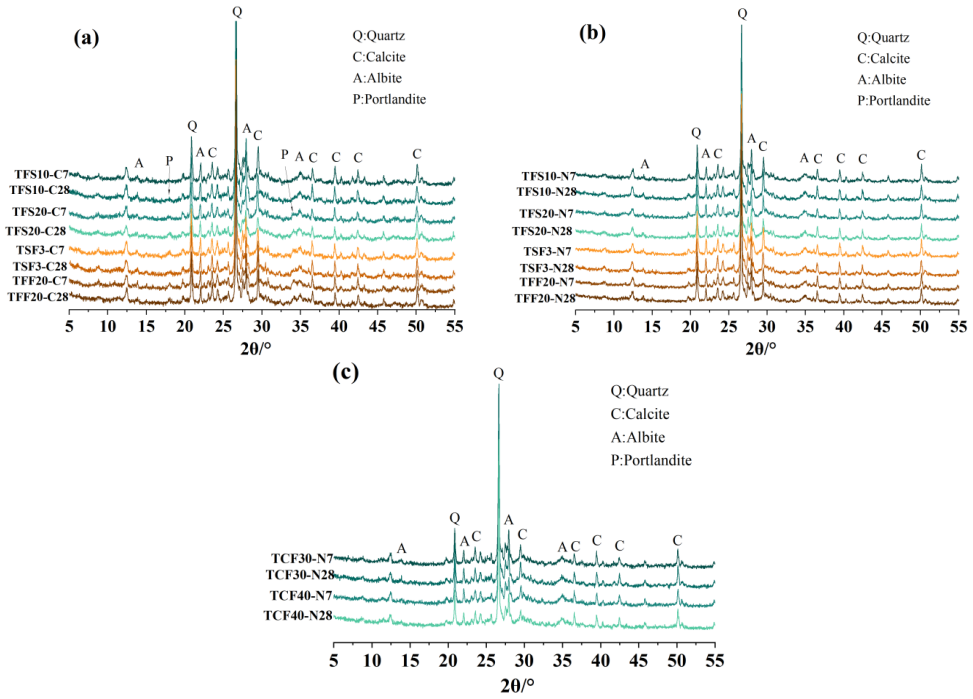

Figure 3. XRD patterns of samples activated by (**a**) calcium hydroxide and (**b**,**c**) sodium hydroxide.

3.3. Thermogravimetric Analysis

To further clarify the differences in the development of compressive strength among all groups, TGA experiments were conducted, and the content of chemical-bound water was calculated based on the TGA results. The TG and DTG curves of samples which were activated by calcium hydroxide are shown in Figure 4. It was observed from Figure 4a that mass loss occurred at various temperatures for samples. According to the DTG curve in Figure 4b, it was found that the intensity of the C-S-H gel decomposition peak in TFS20-C and TFF20-C was the largest within the temperature range of 70 °C to 130 °C [35], which meant that they generated more C-S-H gel during the hydration process. And from Table 3, the chemical-bound water content of both was 4.71% and 4.80%, respectively, at 28 days, higher than that of TSF10-C and TSF3-C, which explained why they had higher compressive strength. In addition, there was a decomposition peak of portlandite in the range of 400 °C to 500 °C [36] in all samples at 7 days, and a reduction of intensity was observed as the curing days went by. The last weight loss in the temperature range of 700 °C to 800 °C indicated the decarbonation of calcium carbonate [36].

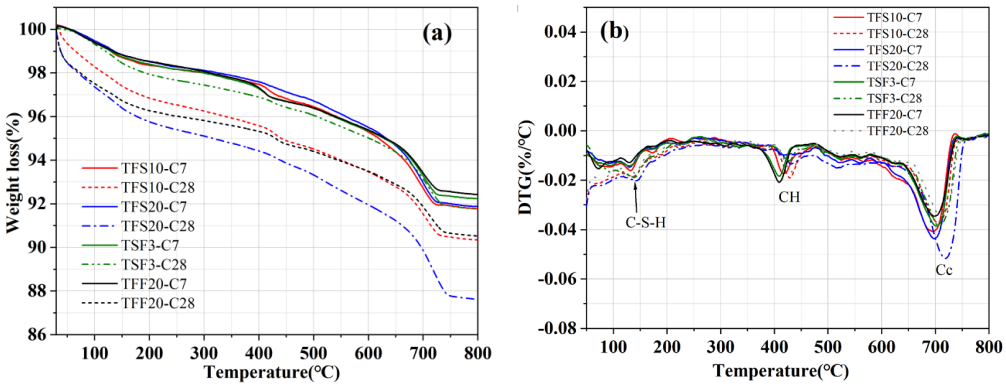

Figure 4. TG and DTG curves of samples activated by calcium hydroxide. (C-S-H: calcium silicate hydroxide; CH: calcium hydroxide; Cc: calcite.) (**a**) TG curves of TFS10, TFS20, TSF3 and TFF20. (**b**) DTG curves of TFS10, TFS20, TSF3 and TFF20.

Table 3. Chemical-bound water (%).

Time	Sample ID				
	TFS10-C	**TFS20-C**	**TSF3-C**	**TFF20-C**	**TFS10-N**
7 d	4.18	4.42	4.33	4.38	4.66
28 d	4.57	4.71	4.59	4.80	5.01
Time	TFS20-N	TSF3-N	TFF20-N	TCF30-N	TCF40-N
7 d	5.36	4.37	5.44	5.73	6.13
28 d	5.50	4.67	5.64	6.31	6.51

The thermogravimetric analysis results of the samples activated by sodium hydroxide are illustrated in Figure 5. The content of C-S-H gel in TFS20-N and TFF20-N increased as the curing days went by, and the chemical-bound water reached 5.50% and 5.64%, respectively, after curing for 28 days. On the contrary, there was little change in TFS10-N and TSF3-N, which indicated that the degree of hydration was very low from 7 days to 28 days. From Figure 5c,d, it was observed that TCF30-N and TCF40-N generated the most C-S-H gel during hydration, and the value of the chemical-bound water was 6.31% and 6.51%, respectively, which was due to an increase in active components. Hence, these samples obtained the highest compressive strength.

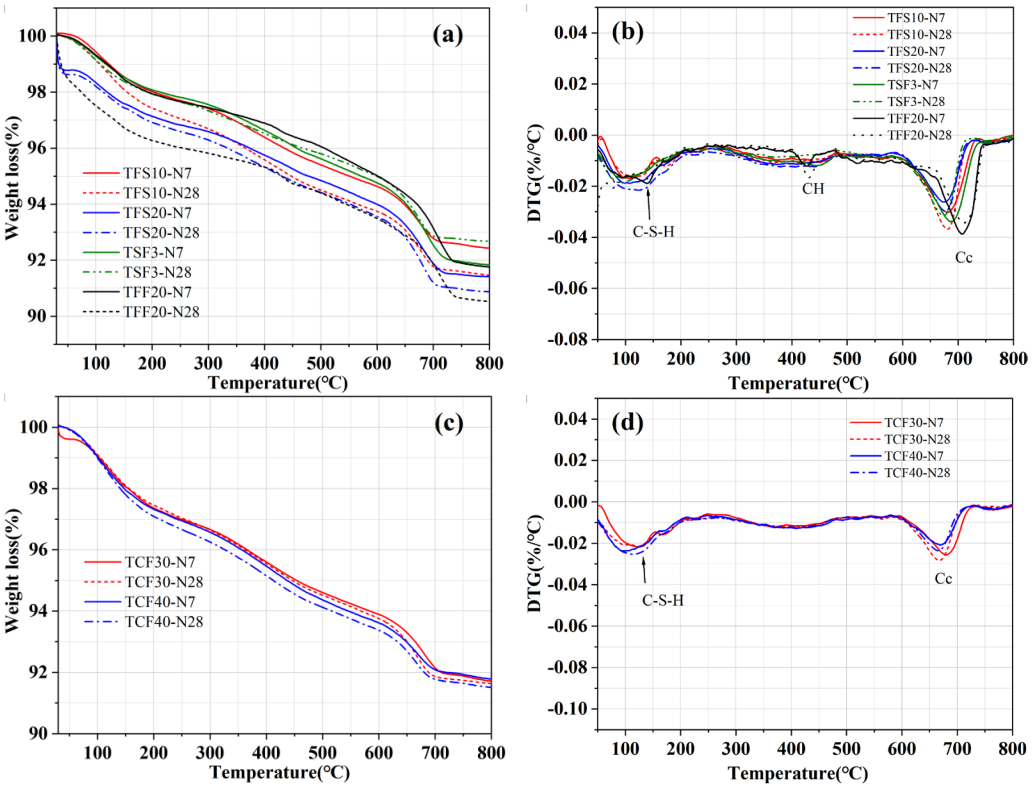

Figure 5. TG and DTG curves of samples activated by sodium hydroxide. (**a**) TG curves of TFS10-N, TFS20-N, TSF3-N and TFF20-N; (**b**) DTG curves of TFS10-N, TFS20-N, TSF3-N and TFF20-N; (**c**) TG curves of TCF30-N and TCF40-N; (**d**) DTG curves of TCF30-N and TCF40-N.

3.4. Scanning Electron Microscopy

The microstructure of the sample was analyzed using scanning electron microscopy, as shown in Figure 6. After curing for 28 days, unhydrated slag and tuff powder were observed in TFS20-C, and a small amount of C-S-H gel was found [36], too. On the contrary, there was more C-S-H gel observed on the surface of tuff powder in TFS20-N, which indicated that sodium hydroxide had a better activation effect. The unhydrated

silica fume was found in TSF3-C, but it was well-distributed. In addition, the C-S-H gels were generated on the surface of the slag. There was a little ettringite [33] in TFF20-C, which could not be found in XRD patterns. Compared to TFF20-C, the reaction degree of fly ash in TFF20-N significantly increased, and the C-S-H gel was denser. The results above indicate that the reactivity of tuff powder is relatively low, whether using calcium hydroxide or sodium hydroxide as an alkaline activator. Furthermore, sodium hydroxide had a significant impact on the reactivity of slag and fly ash, which was beneficial to the development of compressive strength of the samples activated by sodium hydroxide.

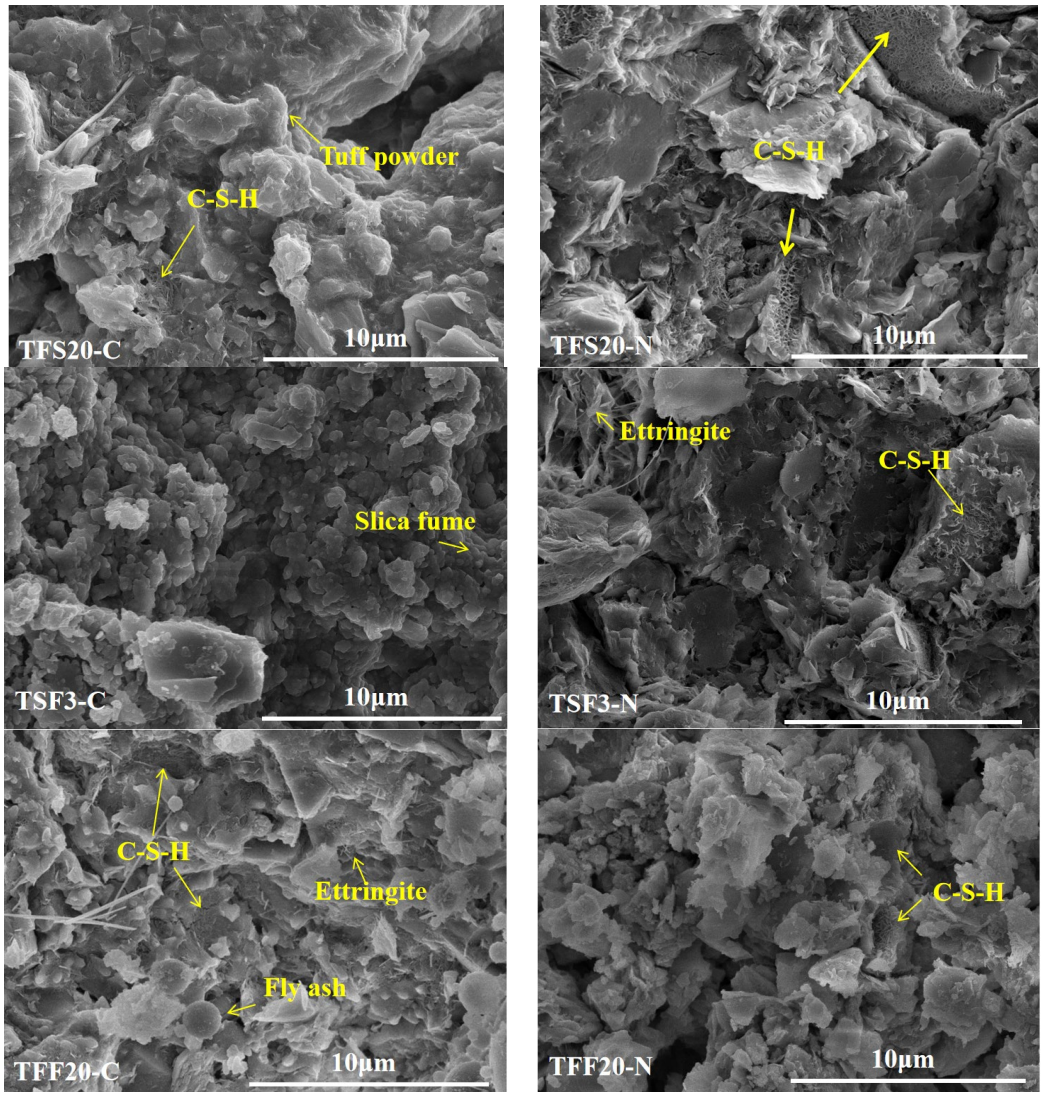

Figure 6. SEM images of sample after curing for 28 days.

3.5. Mercury Intrusion Porosimetry

The properties of building materials are strongly dependent on their pore structure features, including compressive strength and durability [37–39]. Pores are divided into three types based on their size, namely harmless pores (<20 nm), slightly harmful pores (20–50 nm) and harmful pores (50–200 nm) [40] in the field of building materials. The MIP test results are shown in Figure 7, and the porosity within different pore size ranges is counted in Table 4. As shown in Figure 7, the pores of TFF20-N and TCF30-N were mainly distributed in the pore size range of 0 to 100 nm, and those of TFS20-N in the range of 20 to 200 nm. As shown in Table 4, the porosity of TFS20-C and TFF20-C was 26.1% and 25.5%, respectively, and the proportion of harmless pores was 5.4% and 5.2%, respectively.

It was worth noting that there was a 9.6% and 9.0% decrease of porosity in FS20-N and TFF20-N, respectively, compared to TFS20-C and TFF20-C. What was more important was that the sum proportion of harmless pores and slightly harmful pores accounted for 50% and 57.9% of the total porosity in TFS20-N and TFF20-N, respectively, which meant that the samples' pore structure was optimized after activation by sodium hydroxide. What is more, there was a further reduction in TCF30-N's porosity compared to TFS20-N, but the pore distribution was basically consistent.

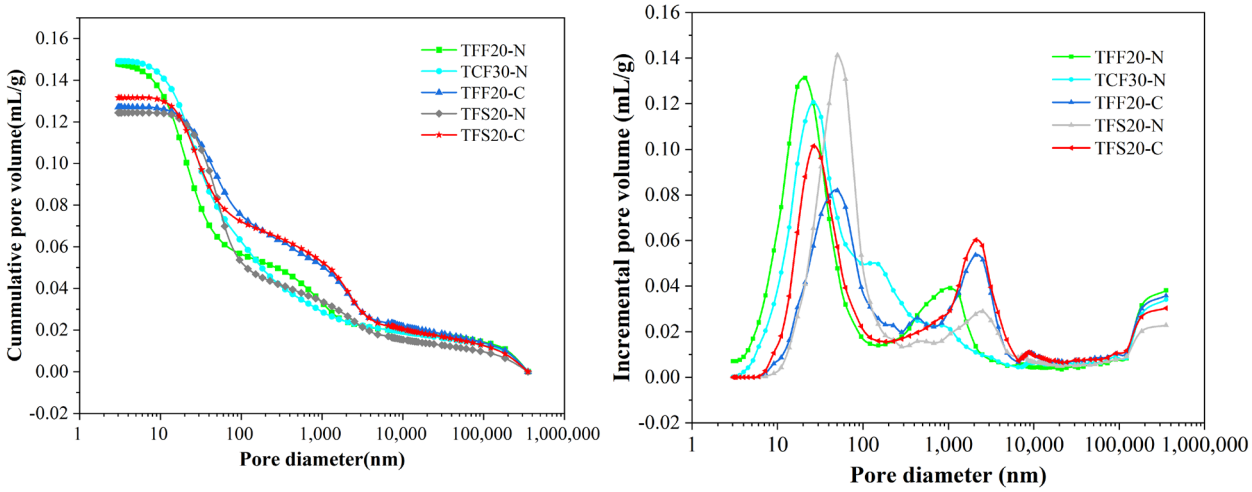

Figure 7. MIP results of sample after curing for 28 days. (**a**), Cumulative pore volume of samples; (**b**), Incremental pore volume of samples.

Table 4. Pore distribution of samples after curing for 28 days (%).

Pore Diameter	Sample ID				
	TFS20-C	**TFF20-C**	**TFS20-N**	**TFF20-N**	**TCF30-N**
1~20 nm	5.4	5.2	5.0	7.1	7.9
20~50 nm	6.3	6.7	6.8	6.1	5.2
50~200 nm	5.4	5.7	6.6	5.5	5.0
>200 nm	9.1	7.8	5.2	4.1	4.2
Total porosity	26.1	25.5	23.6	22.8	22.3

4. Conclusions

This study has investigated the mechanical properties and mechanism of contact-hardening of tuff powder under the method of compression molding. The influencing factors of mechanical properties were explored, and the XRD, TG, SEM, and MIP methods were used to reveal the mechanism of contact-hardening of tuff powder from a microscopic perspective. Based on the above experimental results, the following conclusions are drawn:

(1) There was an increase of compressive strength when the replacement ration of slag increased from 10% to 20%. A further increase happened when tuff powder was replaced by fly ash, but there was little influence when tuff powder was replaced by silica fume, which meant that the role of silica fume in this system was as a filler. When the alkaline activator was changed from calcium hydroxide to sodium hydroxide, the compressive strength of the same mixture proportion at 7 and 28 days was improved. After curing for 28 days, the compressive strength of TFS20 and TFF20 when activated by calcium hydroxide was 12.7 MPa and 12.6 MPa, and when activated by sodium hydroxide it was 15.2 MPa and 15.5 MPa. The compressive strength of TCF30-N and TCF40-N was 21.6 MPa and 23.8 MPa, respectively, which is obviously higher than

the others. It was indicated that the composite systems of two silica-alumina mine solid wastes exhibit better mechanical properties.

(2) The results of XRD showed that there were few hydration products, such as ettringite or calcium hydroxide, after curing for 7 and 28 days in all samples. The results of TGA and SEM indicated that the reason for the increase in compressive strength after replacing calcium hydroxide with sodium hydroxide was that the former had a better activating effect on slag and fly ash. And there were more C-S-H gels and chemical-bound water in TFS20-N and TFF20-N. Hence, the structure of samples was more compacted, and there was a reduction of porosity, especially the proportion of harmful pores. Increasing the replacement ratio of slag or fly ash is an effective measure to improve mechanical properties in this system. Furthermore, the pozzolanic activity of coal gangue powder was better than that of tuff powder. Partially replacing tuff powder with coal gangue powder could improve the mechanical properties of the composite system.

(3) Low-quality silica-alumina mine solid wastes could be compressed into building products with good mechanical properties. It was easy to operate this method with a low energy consumption, which could achieve the reuse of silica-alumina mining resources and reduce carbon emissions in the construction industry. Furthermore, in the follow-up work, on the one hand, the influence of curing conditions on the performance of the system will be studied, and on the other hand, we will search for other types of activators to stimulate the reaction activity of silica-alumina mine solid waste, in order to obtain better performance.

Author Contributions: Conceptualization, B.C. and H.H.; methodology, X.G.; validation, H.H. and P.H.; formal analysis, X.G.; investigation, B.C. and H.H.; resources, X.G. and Y.K.; writing—original draft preparation, B.C.; writing—review and editing, X.G., P.H. and Y.K.; project administration, Y.K. All authors have read and agreed to the published version of the manuscript.

Funding: This research was funded by the CRSRI Open Research Program (Program SN: CKMV2021878/KY) and the National Natural Science Foundation of China (Grant No. 52234004).

Data Availability Statement: The raw data supporting the conclusions of this article will be made available by the authors on request.

Conflicts of Interest: Authors Baojun Cheng, Haoyue Hu, Yaning Kong and Pengyu Huang were employed by the company China West Construction Building Materials Science Research Institute. The remaining authors declare that the research was conducted in the absence of any commercial or financial relationships that could be construed as a potential conflict of interest.

References

1. Lin, B.; Xu, B. Effective ways to reduce CO_2 emissions from China's heavy industry? Evidence from semiparametric regression models. *Energy Econ.* **2020**, *92*, 104974. [CrossRef]
2. Uratani, J.M.; Griffiths, S. A forward looking perspective on the cement and concrete industry: Implications of growth and development in the Global South. *Energy Res. Soc. Sci.* **2023**, *97*, 102972. [CrossRef]
3. Gartner, E.; Sui, T. Alternative cement clinkers. *Cem. Concr. Res.* **2018**, *114*, 27–39. [CrossRef]
4. Habert, G.; Miller, S.A.; John, V.M.; Provis, J.L.; Favier, A.; Horvath, A.; Scrivener, K.L. Environmental impacts and decarbonization strategies in the cement and concrete industries. *Nat. Rev. Earth Environ.* **2020**, *1*, 559–573. [CrossRef]
5. Sharma, M.; Bishnoi, S.; Martirena, F.; Scrivener, K. Limestone calcined clay cement and concrete: A state-of-the-art review. *Cem. Concr. Res.* **2021**, *149*, 106564. [CrossRef]
6. Yu, S.; He, J.; Sang, G.; Yang, S.; Liu, G. Study on hydration process of alkali-activated slag cement activated by weakly alkaline components. *Constr. Build. Mater.* **2024**, *413*, 134716. [CrossRef]
7. Wang, S.D.; Scrivener, K.L.; Pratt, P.L. Factors affecting the strength of alkali activated slag. *Cem. Concr. Res.* **1994**, *24*, 1033–1043. [CrossRef]
8. Cunningham, P.R.; Miller, S.A. Quantitative Assessment of Alkali-Activated Materials: Environmental Impact and Property Assessments. *J. Infrastruct. Syst.* **2020**, *26*, 04020021. [CrossRef]
9. *EN 15743:2010+A1:2015*; Supersulfated—Composition, Specifications and Conformity Criteria, German version. Slovenski Inštitut za Standardizacijo: Ljubljana, Slovenia, 2010. [CrossRef]

10. Matschei, T.; Bellmann, F.; Stark, J. Hydration behavior of sulphate-activated slag cements. *Adv. Cem. Res.* **2005**, *17*, 167–178. [CrossRef]
11. Yao, H. Current situation and development of comprehensive utilization of waste rock resources in metal mines in China. *Chin. J. Nonferrous Met.* **2021**, *31*, 1649–1660. (In Chinese) [CrossRef]
12. Oey, T.; Timmons, J.; Stutzman, P.; Bullard, J.W.; Balonis, M.; Bauchy, M.; Sant, G. An improved basis for characterizing the suitability of fly ash as a cement replacement agent. *J. Am. Ceram. Soc.* **2017**, *100*, 4785–4800. [CrossRef]
13. Thomsen, R.M.; Skibsted, J.; Yue, Y. The Charge-Balancing Role of Calcium and Alkali Ions in Per-Alkaline Aluminosilicate Glasses. *J. Phys. Chem. B* **2018**, *122*, 3184–3195. [CrossRef] [PubMed]
14. Kinnunen, P.; Sreenivasan, H.; Cheeseman, C.R.; Illikainen, M. Phase separation in alumina-rich glasses to increase glass reactivity for low-CO2 alkali-activated cements. *J. Clean. Prod.* **2019**, *213*, 126–133. [CrossRef]
15. Si, Z. *Study on The Influence of Tuff Power Admixture on The Performance of Hydraulic Concrete*; Wuhan Changjiang River Scientific Research Institute: Wuhan, China, 2016. (In Chinese)
16. Liu, S.; Fang, P.; Wang, H.; Kong, Y.; Ouyang, L. Effect of tuff powder on the hydration properties of composite cementitious materials. *Powder Technol.* **2021**, *380*, 59–66. [CrossRef]
17. Kitsopoulos, K.P.; Dunham, A.C. Heulandite and mordenite-rich tufts from Greece: A potential source for pozzolanic materials. *Mineral. Depos.* **1996**, *31*, 576–583. [CrossRef]
18. Yu, Z.; Zhang, T.; Deng, Y.; Han, Y.; Zhang, T.; Hou, P.; Zhang, G. Microstructure and mechanical performance of alkali-activated tuff-based binders. *Cem. Concr. Compos.* **2023**, *139*, 105030. [CrossRef]
19. Lu, X.; Pei, L.; Peng, S.; Li, X.; Chen, J.; Chen, C. Hydration, Hardening Mechanism, and Performance of Tuff Normal Concrete. *J. Mater. Civ. Eng.* **2021**, *33*, 04021063. [CrossRef]
20. Abali, Y.; Bayca, S.U.; Targan, S. Evaluation of blends tincal waste, volcanic tuff, bentonite and fly ash for use as a cement admixture. *J. Hazard. Mater.* **2006**, *131*, 126–130. [CrossRef]
21. Hao, Y.; Guo, X.; Yao, X.; Han, R.; Li, L.; Zhang, M. Using Chinese Coal Gangue as an Ecological Aggregate and Its Modification: A Review. *Materials* **2022**, *15*, 4495. [CrossRef]
22. Gao, S.; Zhang, S.; Guo, L. Application of Coal Gangue as a Coarse Aggregate in Green Concrete Production: A Review. *Materials* **2021**, *14*, 6803. [CrossRef]
23. Ma, H.; Zhu, H.; Wu, C.; Chen, H.; Sun, J.; Liu, J. Study on compressive strength and durability of alkali-activated coal gangue-slag concrete and its mechanism. *Powder Technol.* **2020**, *368*, 112–124. [CrossRef]
24. Qiu, J.; Cheng, K.; Zhang, R.; Gao, Y.; Guan, X. Study on the influence mechanism of activated coal gangue powder on the properties of filling body. *Constr. Build. Mater.* **2022**, *345*, 128071. [CrossRef]
25. Guan, X.; Chen, J.; Zhu, M.; Gao, J. Performance of microwave-activated coal gangue powder as auxiliary cementitious material. *J. Mater. Res. Technol.* **2021**, *14*, 2799–2811. [CrossRef]
26. Liu, S.; Jin, J.; Yu, H.; Gao, Y.; Du, Y.; Sun, X.; Qian, G. Performance enhancement of modified asphalt via coal gangue with microstructure control. *Constr. Build. Mater.* **2023**, *367*, 130287. [CrossRef]
27. Li, J.; Cao, Y.; Sha, A.; Song, R.; Li, C.; Wang, Z. Prospective application of coal gangue as filler in fracture-healing behavior of asphalt mixture. *J. Clean. Prod.* **2022**, *373*, 133738. [CrossRef]
28. Glukhovsky, V.D.; Runova, R.F.; Maxunov, S.I. *Contact-Hardening Cementitious Materials and Compounds*; Chongqing University Press: Chongqing, China, 2004.
29. Wang, S.; Peng, X.; Tao, Z.; Tang, L.; Zeng, L. Influence of drying conditions on the contact-hardening behaviours of calcium silicate hydrate powder. *Constr. Build. Mater.* **2017**, *136*, 465–473. [CrossRef]
30. Wang, S.; Peng, X.; Tang, L.; Ji, G.; Zeng, L. Influence of moisture content on the contact-hardening properties of calcium silicate hydrate by direct compression. *Constr. Build. Mater.* 2021; 278, 122374. [CrossRef]
31. *GB/T 2847-2022*; Pozzolanic Materials Used for Cement Production. State Administration for Market Regulation and Standardization Administration: Beijing, China, 2022.
32. De Weerdt, K.; Haha, M.B.; Le Saout, G.; Kjellsen, K.O.; Justnes, H.; Lothenbach, B. Hydration mechanisms of ternary Portland cements containing limestone powder and fly ash. *Cem. Concr. Res.* **2011**, *41*, 279–291. [CrossRef]
33. Lv, X.; Yang, L.; Li, J.; Wang, F. Roles of fly ash, granulated blast-furnace slag, and silica fume in long-term resistance to external sulfate attacks at atmospheric temperature. *Cem. Concr. Compos.* **2022**, *133*, 104696. [CrossRef]
34. Köhler, S.; Heinz, D.; Urbonas, L. Effect of ettringite on thaumasite formation. *Cem. Concr. Res.* **2006**, *36*, 697–706. [CrossRef]
35. Pane, I.; Hansen, W. Investigation of blended cement hydration by isothermal calorimetry and thermal analysis. *Cem. Concr. Res.* **2005**, *35*, 1155–1164. [CrossRef]
36. Karen, R.S.S.; Lothenbach, B. *A Practical Guide to Microstructural Analysis of Cementitious Materials*; CRC Press: Boca Raton, FL, USA, 2016. [CrossRef]
37. Li, Y.; Wang, P.; Wang, F.; Zheng, X.; Gao, Y. Compressive strength and composite pore structure parameters of iron ore tailings ball concrete. *Constr. Build. Mater.* **2022**, *347*, 128611. [CrossRef]
38. Han, X.; Feng, J.; Wang, B. Relationship between fractal feature and compressive strength of fly ash-cement composite cementitious materials. *Cem. Concr. Compos.* **2023**, *139*, 105052. [CrossRef]

39. Abdel, S.E.R. Exploring damping characteristics of composite tower of cable-stayed bridges. *Sādhanā* **2016**, *41*, 337–344. [CrossRef]
40. Wu, Z. *High Performance Concrete*; Railway Publishing House: Beijing, China, 1999. [CrossRef]